Technical Article

SIMULATION AND ANALYSIS OF GROUNDING SYSTEMS USING THE FINITE ELEMENT METHOD

***Abstract* — The main function of grounding is to enable discharging of fault currents into the soil around a grounding system. The most common approach for dimensioning of the grounding systems is the use of the Finite Element Method (FEM). This paper shows the use of FEM for a static/stationary and first/second order time dependent electromagnetic field problem around grounding systems. Ionization in the soil should also be considered in the numerical model. The parameters of the soil can be obtained using soil models and stochastic methods for the soil models parameters` determination. The applied programme solution is suitable for any grounding system and soil properties, as well as time-varying fault current.**

I. PROBLEM DESCRIPTION

The main function of grounding is to enable discharging of fault currents into the soil around a grounding system (GS) and efficient distribution of potential on the earth surface with purposes of:

- Protection of buildings and installations against lightning,
- Safety of human and animal life by limiting touch and step voltages to safe values,
- Electromagnetic compatibility (EMC).

An analysis of the conditions in the vicinity of a grounding system, when the fault current flows through a conductor which connects the above-ground and underground parts of the GS, requires the calculation of the electromagnetic field. The problem seems simple at first view. The computation space consists of a low-conductive part, soil in which the grounding is buried made of high conductive material, and of the air above the surface of the soil. The geometries of individual domain are usually simple, the electric and magnetic properties of the domain are linear, except in the case of the ionization of the soil.

Thus, the electric conductivity σ_{GS} of the GS is constant, in the range of 10^6 S/m to 10^7 S/m, and the soil conductivity σ_s is approximately in the range of 0.1 S/m to 0.0005 S/m [1, 2]. The structure of the soil can be very different, so the calculation must be done for the cases in which the soil is:

- Homogeneous,
- Layered and homogeneous in layers,
- Partly locally inhomogeneous:
  - Due to the protected objects, or objects in the vicinity of the GS, whose parts (reinforced concrete) are located in the ground,
  - Due to the need to improve the conductivity of the soil in the immediate proximity of the GS (gels, layers of good conducting soil, …),
  - Due to the configuration of the terrain (stone parts in the surroundings, water resources, …),
  - Due to the soil ionization at higher $\boldsymbol{J}$, when conductivity becomes a nonlinear function of $\boldsymbol{E}$ or $\boldsymbol{J}$. A more precise model (i.e. dynamic model of ionization) contains a hysteresis dependence $\sigma(\boldsymbol{J})$.

The presented general problem of the GS is described by the full system of Maxwell's equations (1).

$$\left.\begin{aligned} \operatorname{curl}\boldsymbol{H} &= \boldsymbol{J} + \frac{\partial \boldsymbol{D}}{\partial t} \\ \operatorname{curl}\boldsymbol{E} &= -\frac{\partial \boldsymbol{B}}{\partial t} \\ \operatorname{div}\boldsymbol{B} &= 0 \\ \operatorname{div}\boldsymbol{D} &= \rho \end{aligned}\right\} \Rightarrow \quad \operatorname{div}\boldsymbol{J} = -\frac{\partial \rho}{\partial t} \tag{1}$$

In practice, we distinguish two separate examples:

I. Consideration of the conditions in the vicinity of the GS, when a fault current occurs during the operation of the power system of the frequency 50 Hz or 60 Hz, or when a failure occurs in a DC circuit. The current field in the soil, which is a consequence of such a failure, is written completely by (2), and can be considered as a stationary (or static) current field. Using the electric potential φ, a problem can be written by 2nd order PDE (Laplace's equation) [6-13]. The main parameters of the calculation are the distribution of the electric potential, step voltage U_s and touch voltage U_t at the surface of the soil, and grounding resistance R.

$$\begin{aligned} \operatorname{curl}\boldsymbol{E} &= 0 \\ \operatorname{div}\boldsymbol{J} &= 0 \\ \boldsymbol{J} &= [\sigma]\boldsymbol{E} \end{aligned} \tag{2}$$

II. Consideration of the conditions in the vicinity of the GS when the pulse current flows into the soil (for example in the case of lightning strike in the over ground part of the GS). The electromagnetic field in the soil and in the air above the ground is described with the complete system of (1). Using magnetic vector potential $\boldsymbol{A}$ and electric scalar potential φ, the problem is described by a system of two wave or diffusion equations. The main parameters of the calculation are the grounding (pulse) impedance, the distribution of the electric potential, U_s and U_t at the surface of the soil, all as a function of time, as well as the electromagnetic field (EMF) in the air and in the vicinity of the GS.

TABLE I. INPUT DATA FOR THE STATIONARY (STATIC) AND TRANSIENT FIELD CALCULATION OF GS USING FEM.

Static calculation				Ionization		
Soil	$\sigma=\sigma_s$	/	/	σ_{ion}=const.	/	/
GS	$\sigma=\sigma_{GS}$	/	/		/	/

Transient calculation				Ionization		
Soil	$\sigma=\sigma_s$	$\mu=\mu_0$	ε=(1-80) ε_0	$\sigma=\sigma(\boldsymbol{J})$	T_i	T_d
Air	σ=0	$\mu=\mu_0$	$\varepsilon=\varepsilon_0$	/	/	/
GS	$\sigma=\sigma_{GS}$	$\mu=\mu_0$	/	/	/	/

Although different approaches [25-36] have been developed through the development of the GS solving, for example:

- Circuit approach,
- Transmission line approach,
- Hybrid approach,
- Electromagnetic field approach:

- Method of Moment (MoM),
- Partial Element Equivalent Circuit (PEEC) method,
- Finite Difference Time Domain method (FDTD),
- Finite Element Method (FEM).

From the description of the general problem, it follows that FEM is the most appropriate method for the EMF calculation in the vicinity of the GS. If we are more precise, it should be mentioned that, even when using FEM, we meet restrictions at solving these problems. We must be aware of these restrictions and, using an appropriate approach, their influence on the calculation's accuracy should be minimised. The first restriction is that the problem is half-infinite (for static calculation or at low frequencies), or infinite at transient calculation. There are different approaches from the finite boundary to the appropriate mapping, Absorbing Boundary Conditions (ABC), perfect matched layer (PEC/PLM) or combination FEM and Boundary Element Method (BEM), which is treated extensively in the relevant literature [6-11, 35]. Other limitations are the large relationship between the conductivity of the GS and the conductivity of the soil (in the range of 10^7 to 10^{11}), which, in combination with very small cross-sections of the conductors and GS rods, present a problem at discretization of the space. In particular, this is important in the case of transient calculation, due to the skin effect and stability of the calculation procedure. Because of the time integration (13) or (15) which is used for the whole injected current wave, the calculation procedure is a time-consuming process.

For this reason, it is important to make time optimization of the calculation algorithm. Inclusion of parallel processing and/or use of a graphical processing unit are two approaches which enable much shorter calculation time.

The precise calculation of the GS is also conditioned by good knowledge of the input data. The geometry and electrical properties of the GS are well known, the greater problem is the knowledge of the physical properties of the soil (especially σ and ε, and, in the case of soil ionization, also knowledge of the ionization model parameters E_c, T_i and T_d). The basic step in determining the properties of the soil in the vicinity of the particular GS is, however, the determination of its conductivity, which is reduced to the determination of the N layered equivalent soil model. The equivalent model is determined with the help of the appropriate measurement, usually Wenner's method [2, 14] in combination with the numerical or graphical process. In fact, this is an inverse approach for the determination of the conductivity and layer thicknesses of the soil presented in the equivalent soil model used for the calculation. Due to the mentioned approach of obtaining input data for the calculation, it is necessary to be aware of the effect of the equivalent soil model on the final calculation accuracy considering the concrete case. Additionally, inhomogeneities in the soil structure influence the calculation accuracy if they are not taken into account. As mentioned, the equivalent soil model is obtained from measurements using an inverse approach. Different procedures were used in this process, from graphic, analytical, to various optimization algorithms; either deterministic, or stochastic.

II. Soil Parameters Determination Using the Stochastic Approach

As described, we are dealing with an inverse problem. Two and multi-layered horizontal analytical models were developed in the past [3]. Mainly, two and three-layered soil models are in use. We tested the two-layered (I2), the simplified two-layered and the three-layered models (I3). We tried to find which of the tested models is the most appropriate, and to determine the best metaheuristics [15] among the tested models for the determination of the soil parameters.

The search for the soil parameters that best fit the measurement data is an optimization problem. In the literature different approaches can be found, which present soil parameters' determination using different standard optimization methods [20], and, in the present period, soil parameters' determination works using modern metaheuristics [21]. We used different metaheuristics. For all of them, it is common that they are robust and that they can avoid local minima.

We compared different metaheuristics using three different soil models. Our choice was the oldest Genetic Algorithm (GA) [18] and four state-of-the-art methods, which are Differential Evolution (DE) [21, 22], Teaching-Learning Based Optimization (TLBO) [19], Artificial Bee Colony (ABC) [16] and self-adaptive Differential Evolution Algorithm (jDE) [17]. During the tests, we found that the two-layered model was not appropriate for all test data and, consequently, the three-layered model is more appropriate to be used as a general soil model [23].

Concerning solving methods, we also found out that TLBO was very stable, and almost the same quality result was obtained after each run. On the other hand, for some test examples, all tested methods except ABC are stuck in a local minimum, and they were able to avoid the local minimum only in some runs. With the aim to overcome local minima and to obtain stability of TLBO, we combined ABC and TLBO, and obtained a method marked as ABCandTLBO [23]. The calculation is started using ABC and, after that, the best solution from ABC is used as one of the initial values in TLBO. The presented solution, the selected three-layered model, together with the soil parameters' determination method ABCandTLBO, is appropriate to be used together with, or as a part of the FEM software, which is suitable for the design of the grounding systems.

One of the typical calculated soil parameters (using ABCandTLBO) of the two and three-layered models, together with calculated specific resistivity based on the presented models, compared with measurements which are the basis for the calculation, is presented in Fig. 1 [23].

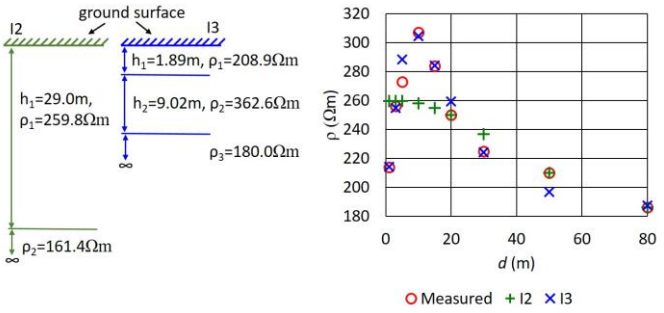

Fig. 1. Soil parameters of two and three layered model together with calculated and measured specific resistivity.

Due to the approach of these algorithms, where the population of the solution within each iteration needs to be evaluated, the time spent for the calculation is long. Therefore, an approximate analytical formula for the calculation of the resistance between the two electrodes used in the measurements is used to evaluate the target (fitness) function. This, additionally, affects the accuracy of the obtained

equivalent soil model. A more precise approach will certainly be obtained with use of the numerical methods, for example, FEM to evaluate fitness function, but this would increase the calculation time for the determination of the equivalent soil model drastically.

III. Numerical Models

A. FEM Model of Static (Stationary) Field

For the analysis of the grounding system at industrial frequency or at DC conditions we use (2). With help of these equations, the electric scalar potential φ, presented in (3), can be introduced.

$$\boldsymbol{E} = -\nabla\varphi \tag{3}$$

When (3) is inserted into (2) we obtain the mathematical model of the problem described by the Laplace's equation:

$$\nabla\left([\sigma]\nabla\varphi\right) = 0, \tag{4}$$

where $[\sigma]$ is the tensor of soil conductivity. The current field in the soil Ω is described entirely by (4), when the boundary conditions (5) on boundary Γ are known.

$$\varphi = 0 \ (r \to \infty), \ \frac{\partial\varphi}{\partial n} = 0 \ \text{(on the earth surface)} \tag{5}$$

By applying the Galerkin's formulation of FEM [3, 4], the additional transformation of the "semi-infinite space" [6-8], the 3D finite element for soil discretization, and the 1D finite element for the grounding system [9, 10], the final form of the FEM equation of the grounding system represents the system of equations (6), whose solutions are the values of φ in all nodes of finite element mesh.

$$[\boldsymbol{A}]\{\varphi\} = \{\boldsymbol{B}\} \tag{6}$$

The above approach is useful for most cases involving any GS geometry and a multi-layer soil model with additional local inhomogeneity in the soil. The influence of different layers of the soil and of the local inhomogeneity is illustrated at example 2. Figure 2 shows the grounding grid, which is buried in two-layer soil, at a depth of 0.8 m.

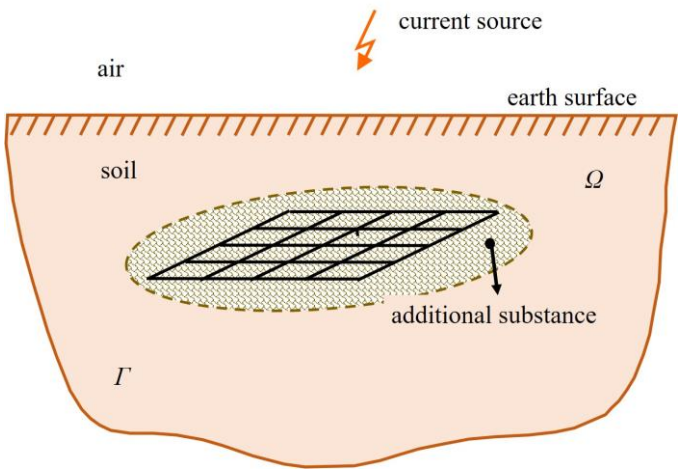

Fig. 2. Grounding grid and additional substance in soil.

Due to the need to reduce operational ground resistance, the soil in the immediate vicinity of the GS is replaced by an additional substance with better resistivity (50 Ωm) than the soil resistivity (200/800 Ωm).

To evaluate the influence of an additional substance on the grounding grid parameters, we have studied three different kinds of soil structure models [13]. Model A corresponds to a single-layer (or uniform) soil model with resistivity of 200 Ωm, model B corresponds to a uniform soil model with resistivity of 1000 Ωm, and model C corresponds to a horizontal two-layer soil model with first-layer resistivity (from the earth`s surface to a depth of 4 m) of 200 Ωm and second-layer resistivity of 800 Ωm.

In each case, the calculations for various thicknesses of soil layers impregnated with an additional substance embedding the grounding grid were carried out. All cases without the presence of additional substance are numerated with index 1. All cases with the presence of additional substance of 0.2 m above and 0.05 m below the grounding grid are numerated with index 2. Finally, all cases with the presence of additional substance of 0.4 m above and 0.15 m below the grounding grid are numerated with index 3.

In the following pictures, the calculated results of the earth`s surface potential, variations along the diagonal of the grid are shown respectively. The results of grounding grid potential and ground resistance obtained for different thicknesses of additional substance are presented in Fig. 3 – Fig. 6.

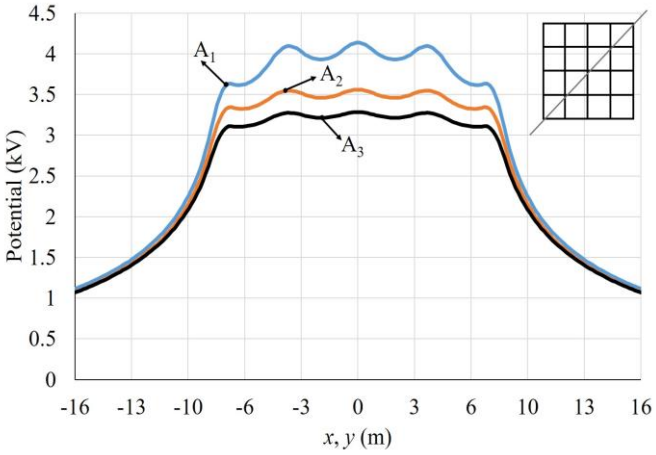

Fig. 3. Distribution of earth surface potentials due to various thicknesses of additional substance in a uniform soil model A.

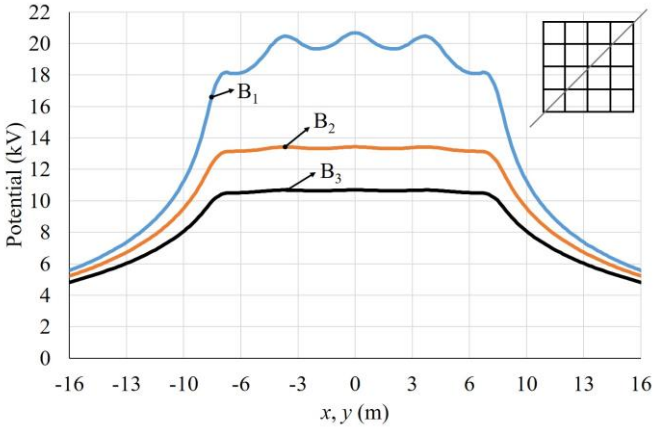

Fig. 4. Distribution of earth surface potentials due to various thicknesses of additional substance in a uniform soil model B.

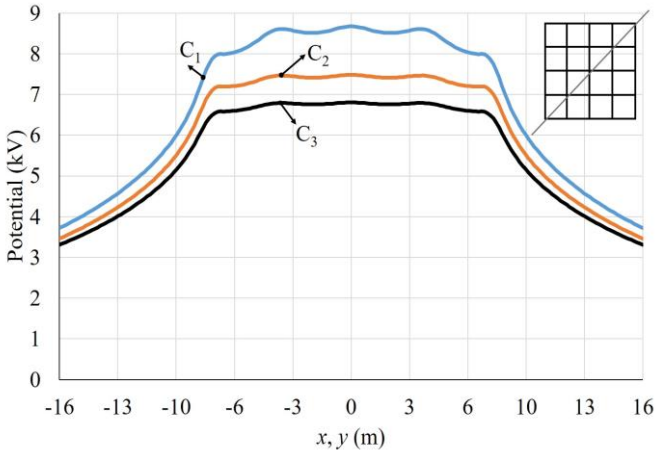

Fig. 5. Distribution of earth surface potentials due to various thicknesses of additional substance in a two-layer soil model C.

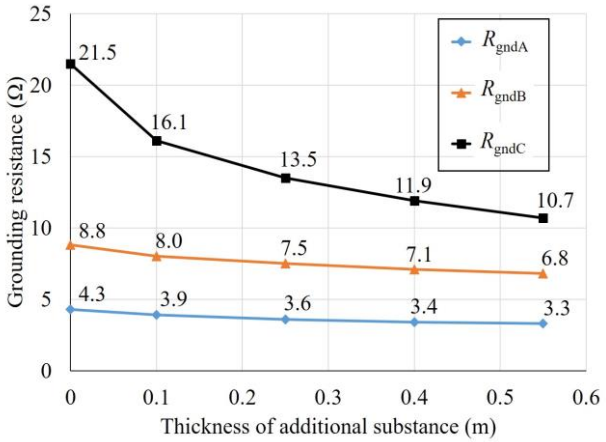

Fig. 6. The influence of soil resistivity and thickness of additional substance on grounding resistance.

In cases, where we also want to include the ionization effect into the numerical model, the problem becomes nonlinear, because it is now $\sigma(\boldsymbol{E})$ or $\sigma(\boldsymbol{J})$, and it is necessary to solve (6) iteratively. For that, it is necessary to consider that the influence of the soil ionization is taken into account only by the step change of the soil conductivity in the part of the soil where the condition $\boldsymbol{E}>\boldsymbol{E}_c$ (or $\boldsymbol{J}>\boldsymbol{J}_c$) is fulfilled. The conductivity of the ionized soil in this part is usually set to a value equal to the conductivity of the grounding [42-45], which is, of course, overestimated. The more realistic assumption is that, in the ionized soil, the conductivity value is a certain percentage of the initial soil conductivity. A precise determination of this value is highly questionable, since various experimental results are also very varied [47].

The effect of soil ionization on the characteristic of the GS is presented for the example of a single steel rod with length of 1 m and radius of 25 mm, shown in [44]. The grounding rod was placed vertically from the earth surface into uniform soil with the resistivity of 43.5 Ωm. The measured value of grounding resistance was 23.2 Ω, which differs slightly from the computed value in [42], which was 25.4 Ω, and a bit more from our computed value, obtained by FEM, which was 28 Ω. Table II summarises the computed values obtained from the mathematical model based on circuit theory and from our suggested model based on FEM (COMP FEM), as well as the results of measurements (MEA) performed on the vertically buried steel rod.

TABLE II. MEASURED AND COMPUTED RESULTS FOR THE VERTICAL ROD.

I_{max} (kA)	GPR (kV)			R (Ω)		
	MEA	COMP [42]	COMP FEM	MEA	COMP [42]	COMP FEM
5.2	92	95.1	86.9	17.692	18.28	16.71
10.5	137	147.3	134	13.048	14.03	12.76
21.4	200	212.7	211.3	9.346	9.94	9.872
27.2	230	236	241.4	8.456	8.68	8.873
30.8	248	248.3	261	8.052	8.06	8.475

In Fig. 7, for the grounding rod under test, the distribution of the grounding resistance is shown as a function of maximum values of injected current with reference to the measurements and computations executed in [42], as well as to the computations performed by FEM.

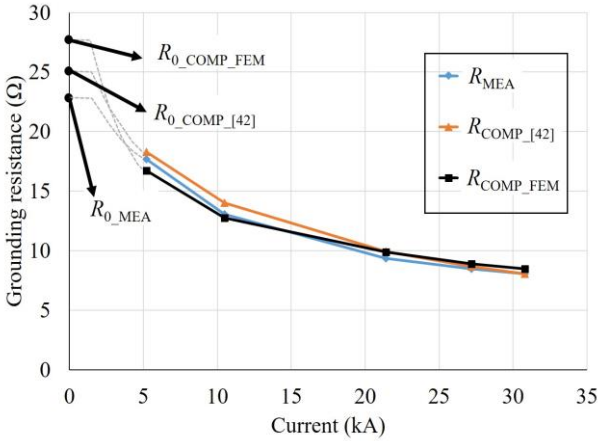

Fig. 7. Measured and calculated grounding resistance as a function of the maximum value of the current injected into the vertical rod.

As was to be expected, the grounding resistance decreases if soil ionization around the grounding rod occurs. The good agreement between the measurements and the numerical results shows the validity of our proposed method and permits us to confirm that our model simulates the soil ionization phenomenon in a quite accurate way. Fig. 8, Fig. 9 and Fig. 10 present the earth surface potential response of the grounding rod, subjected to various values of injected current.

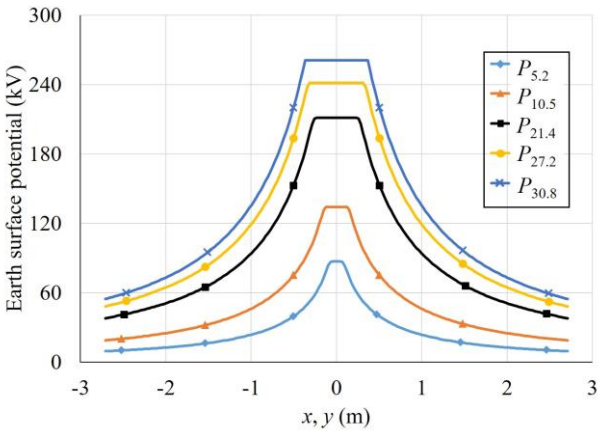

Fig. 8. Earth surface potential variations along the line above the vertical rod excited by high magnitude currents considering the soil ionization effect.

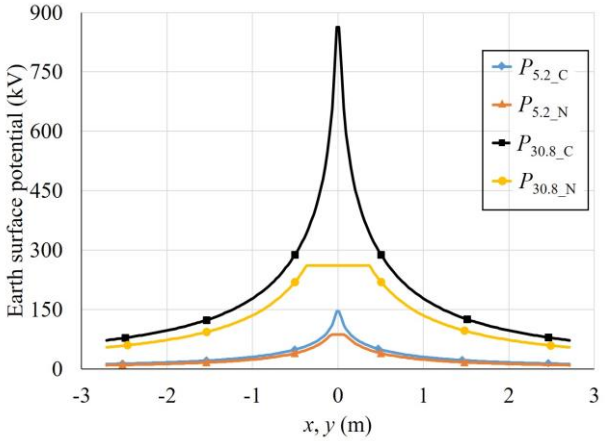

Fig. 9. Comparison between earth surface potential distributions above a vertical rod, excited by 5.2 kA and 30.8 kA current magnitudes, in the case of considering and not considering the soil ionization effect.

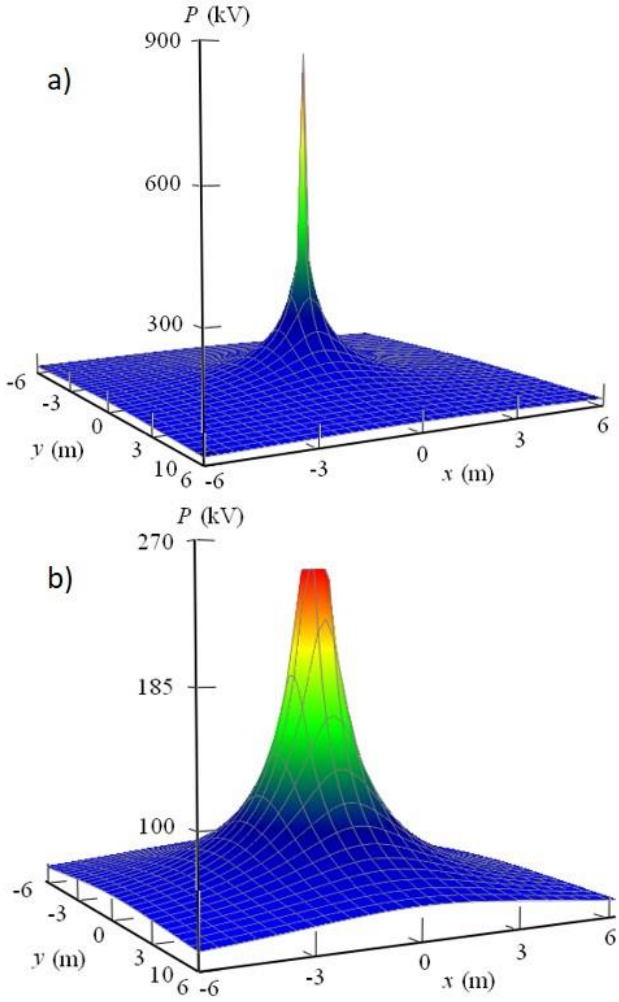

Fig. 10. 3D earth surface potential distributions above a vertical rod, excited by 30.8 kA current magnitudes, in the case of not considering (a) and considering (b) the soil ionization effect.

B. FEM Model of Transient Electromagnetic Field

The governing partial differential equations for transient problems of GS can be derived from Maxwell's equations (1). When magnetic vector potential $\boldsymbol{A}$, electric scalar potential φ, conduction and displacement current are introduced to the calculated domain, the following equations are obtained:

$$\nabla\times\frac{1}{\mu}\nabla\times\boldsymbol{A}-\nabla\frac{1}{\mu}\nabla\boldsymbol{A}+ +\sigma\left(\frac{\partial\boldsymbol{A}}{\partial t}+\nabla\varphi\right)+\varepsilon\left(\frac{\partial^2\boldsymbol{A}}{\partial t^2}+\nabla\frac{\partial\varphi}{\partial t}\right)=0 \tag{7}$$

$$\nabla\cdot\left[\sigma\left(\frac{\partial\boldsymbol{A}}{\partial t}+\nabla\varphi\right)+\varepsilon\left(\frac{\partial^2\boldsymbol{A}}{\partial t^2}+\nabla\frac{\partial\varphi}{\partial t}\right)\right]=0 \tag{8}$$

Equation (8) defines a divergence of the total current density ($\boldsymbol{J}_{\text{tot}}$), which consists of two components: Conduction current density $\boldsymbol{J}_{\text{cond}}$ (9a) and displacement current density $\boldsymbol{J}_{\text{disp}}$ (9b).

$$\boldsymbol{J}_{\text{cond}}=\sigma\left(-\frac{\partial\boldsymbol{A}}{\partial t}-\nabla\varphi\right) \tag{9a}$$

$$\boldsymbol{J}_{\text{disp}}=\varepsilon\left(-\frac{\partial^2\boldsymbol{A}}{\partial t^2}-\nabla\frac{\partial\varphi}{\partial t}\right) \tag{9b}$$

Where μ is the permeability, σ the electrical conductivity and ε is the permittivity. Equations (7) and (8) already contain the Coulumb's gauge to ensure the unique solution to the magnetic vector potential $\boldsymbol{A}$, which is given in greater detail in [24]. By applying the finite elements procedure and weighted residual method [3, 4], the following equation is obtained (10).

$$\int_{\Omega}\left[\frac{1}{\mu}\nabla\times\boldsymbol{N}_{\text{i}}\nabla\times A+\frac{1}{\mu}\nabla\boldsymbol{N}_{\text{i}}\nabla\boldsymbol{A} +\sigma\boldsymbol{N}_{\text{i}}\frac{\partial\boldsymbol{A}}{\partial t}+\sigma\boldsymbol{N}_{\text{i}}\nabla\varphi+\varepsilon\boldsymbol{N}_{\text{i}}\frac{\partial^2\boldsymbol{A}}{\partial t^2}+\varepsilon\boldsymbol{N}_{\text{i}}\nabla\frac{\partial\varphi}{\partial t}\right]\text{d}\Omega=0 \tag{10}$$

The described problem is an open boundary problem. Various techniques can be used to include the infinite region in the calculation, as shown in [6-11, 35].

The final FEM equation is represented by a system of second order ordinary differential equations (11), where V (12) represents the modified electric scalar potential [24], in order to ensure that matrices $\boldsymbol{K}$, $\boldsymbol{C}$ and $\boldsymbol{M}$ are symmetrical.

$$[\boldsymbol{K}]\begin{Bmatrix}\boldsymbol{A}\\V\end{Bmatrix}+\sigma[\boldsymbol{C}]\begin{Bmatrix}\dot{\boldsymbol{A}}\\\dot{V}\end{Bmatrix}+\varepsilon[\boldsymbol{M}]\begin{Bmatrix}\ddot{\boldsymbol{A}}\\\ddot{V}\end{Bmatrix}=0 \tag{11}$$

$$\varphi=\frac{\partial V}{\partial t}=\dot{V} \tag{12}$$

The column vector of unknown nodal potentials in (11) is {$\boldsymbol{A}$, V}. The next column vectors are the first and second derivative of nodal potentials and $\boldsymbol{K}$, $\boldsymbol{C}$, $\boldsymbol{M}$ are corresponding matrices, which are linked with the potentials $\boldsymbol{A}$ and V and the Laplacian operator ($\boldsymbol{K}$), with the conduction current ($\boldsymbol{C}$) and with the displacement current ($\boldsymbol{M}$).

Time integration (13) can be conducted with different time-step algorithms, such as Newmark's, Crank-Nicolson's, Wilson's and others [3, 4]. With an assumption of linear interpolation throughout time, the following recursive equation (13) is obtained from (11):

$$\left[\left(f_{\mathrm{M}}+\frac{1}{\theta\Delta t}\right)[\boldsymbol{M}]+\theta\Delta t[\boldsymbol{K}]\right]\begin{Bmatrix}\boldsymbol{A}^{(n+1)}\\ V^{(n+1)}\end{Bmatrix}=$$
$$=\left[\left(f_{\mathrm{M}}+\frac{1}{\theta\Delta t}\right)[\boldsymbol{M}]\right]\begin{Bmatrix}\boldsymbol{A}^{(n)}\\ V^{(n)}\end{Bmatrix} \qquad (13)$$
$$-\left[(1-\theta)\Delta t[\boldsymbol{K}]\right]\begin{Bmatrix}\boldsymbol{A}^{(n)}\\ V^{(n)}\end{Bmatrix}+\left[\frac{1}{\theta}[\boldsymbol{M}]\right]\frac{d}{dt}\begin{Bmatrix}\boldsymbol{A}^{(n)}\\ V^{(n)}\end{Bmatrix}$$

where parameters f_{M} and θ are given by the following expressions: $f_{\mathrm{M}} = \mu/\varepsilon$ and $0.5 \le \theta \le 1$. The recursive equation (13) enables the calculation of the potentials, in the new time step (n+1), depending on the preceding time step (n). When displacement current is not considered in the calculation, (11) is written in the simpler form (14) as a system of first order ordinary differential equations.

$$[\boldsymbol{K}]\begin{Bmatrix}\boldsymbol{A}\\ V\end{Bmatrix}+\sigma[\boldsymbol{C}]\begin{Bmatrix}\dot{\boldsymbol{A}}\\ \dot{V}\end{Bmatrix}=0 \qquad (14)$$

The time step algorithm (13) is also simplified, which is now written in the form (15).

$$\left[[\boldsymbol{M}]+\theta\Delta t[\boldsymbol{K}]\right]\begin{Bmatrix}\boldsymbol{A}^{(n+1)}\\ V^{(n+1)}\end{Bmatrix}=\left[[\boldsymbol{M}]-(1-\theta)\Delta t[\boldsymbol{K}]\right]\begin{Bmatrix}\boldsymbol{A}^{(n)}\\ V^{(n)}\end{Bmatrix} \qquad (15)$$

In the case of the transient calculation (11) or (14) with consideration of the ionization, the dynamic model of the ionization must also be considered [46-64]. It covers both ionization and deionization processes in the soil, which are initiated at a sufficiently large injected current flow into the soil. The authors of the standard model (Fig. 11) are Liew and Darweniza [46].

Darweniza's model of soil ionization/deionization divides the entire area of the soil into two regions. The first, non-ionization region, represents the neighbourhood of the GS, where the current density $\boldsymbol{J}$ at any point in this region doesn't exceed the value of $\boldsymbol{J}_{\mathrm{c}}$ over the entire duration of the impulse wave (Fig. 11, 0→1).

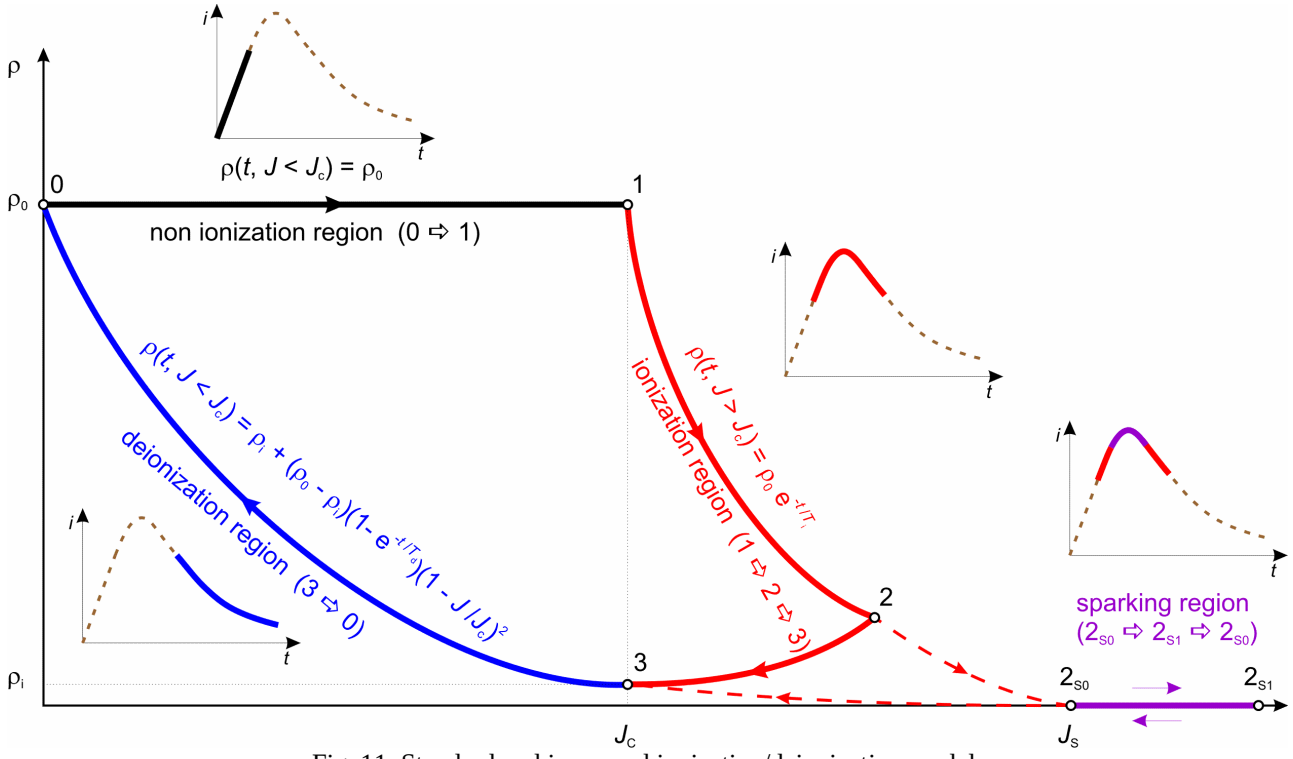

Fig. 11. Standard and improved ionization/deionization model.

The soil resistance does not change during the current pulse, and it is equal to the initial value

$$\rho(t, \boldsymbol{J} < \boldsymbol{J}_{\mathrm{c}}) = \rho_0 \qquad (16)$$

The second ionization region represents the neighbourhood of the GS, where, in a given time interval within the current wave (Fig. 11, 1→2→3), the current density $\boldsymbol{J}$ becomes greater than $\boldsymbol{J}_{\mathrm{c}}$ at all points of the region, and the ionization process is initiated. This affects the change in the soil resistance $\rho(t,\rho_0,\boldsymbol{J}>\boldsymbol{J}_{\mathrm{c}})$. The resistance starts to decrease (17) and falls to the minimum value ρ_{i} through the ionization process (Fig. 11, point 3). Since the time value of the current after reaching the maximum value begins to decrease, also $\boldsymbol{J}$ starts to decrease in all points of this region.

$$\rho(t, \rho_0, \boldsymbol{J} < \boldsymbol{J}_{\mathrm{c}}) = \rho_0 e^{-\frac{t}{T_{\mathrm{i}}}} \qquad (17)$$

When $\boldsymbol{J}$ again decreases below the value of $\boldsymbol{J}_{\mathrm{c}}$ in this region (now it is a deionization region) a reversible deionization process starts, which affects the soil resistivity $\rho(t,\rho_0,\rho_{\mathrm{i}},\boldsymbol{J}<\boldsymbol{J}_{\mathrm{c}})$. It begins to rise again to the initial value in the rest of the impact wave (Fig. 11, 3→0).

$$\rho(t, \rho_{\mathrm{i}}, \rho_0, \boldsymbol{J} < \boldsymbol{J}_{\mathrm{c}}) = \rho_{\mathrm{i}} + (\rho_0 - \rho_{\mathrm{i}})\left(1 - \rho_0 e^{-\frac{t}{T_{\mathrm{d}}}}\right)\left(1 - \frac{\boldsymbol{J}}{\boldsymbol{J}_{\mathrm{c}}}\right)^2 \qquad (18)$$

This ionization model was improved and extended with the work of J. Wang et al. [48]. The essential difference due to the

basic model is that the additional region (the so-called sparking region) is introduced, in which discrete breakdown paths occur on the surface and inside the soil. This phenomenon (Fig. 11, $2_{s0} \rightarrow 2_{s1} \rightarrow 2_{s0}$) is initiated when $\boldsymbol{J}$ becomes larger than $\boldsymbol{J}_s$. The value of ρ of this region is reduced to zero (19).

$$\rho\left(t, \boldsymbol{J} > \boldsymbol{J}_s\right) = 0 \tag{19}$$

The ionization region in the improved model is now defined with the condition $\boldsymbol{J}_c < \boldsymbol{J} < \boldsymbol{J}_s$ (Fig. 11, $1 \rightarrow 2_{s0} \rightarrow 3$), and previously it was $\boldsymbol{J} > \boldsymbol{J}_c$ (Fig. 11, $1 \rightarrow 2 \rightarrow 3$).

In this case, $\boldsymbol{J}_c$ is the value of $\boldsymbol{J}$ when the ionization process in the soil is initiated, and $\boldsymbol{J}_s$ is the value of $\boldsymbol{J}$ when discrete breakdowns and filamentary arc paths occur in the soil. Both values can only be determined experimentally, where different authors specify (quite) different values [46, 48, 65-68].

IV. Case Analysis

The use of the described numerical model for the transient calculation of the GS is presented in the continuation. Analysis is made for the experimental setup (Fig. 12), which assembles the grounding mesh under test with dimensions 6 m x 6 m at a depth of 0.5 m, connected with four vertical rods of 2 m length and auxiliary mesh.

The auxiliary mesh consists of two horizontal conductors of 4 m length at a depth of 0.3 m and four vertical rods of 1.4 m length. The soil is two-layered, with the 1st layer's resistivity of 140 Ωm and depth of 1.9 m, and the 2nd layer's resistivity of 90 Ωm. The current wave is the same in all cases, and it is represented by the double exponential current waveform as $I(t) = 1000\,(e^{-0.015t} - e^{-1.8t})$.

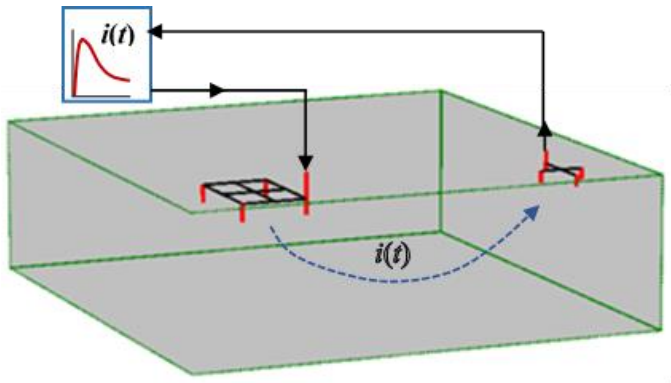

Fig. 12. Experimental setup consisting of impulse generator, mesh under test and auxiliary mesh.

A. Calculation with Consideration of the Soil's Permittivity

The graphs shown in Fig. 13 present the grounding impedance $Z(t)$ without (1st order problem) and with consideration of displacement current (2nd order problem), for two different values of the soil's relative permittivity 15 (Zp15) and 30 (Zp30), without ionization consideration. It can be seen that the inductive and capacitive effect is most pronounced in the initial part of the current pulse, and later the conduction effect is predominant. For this reason, graph $Z(t)$ is shown only for the initial part of the pulse. The inductive effect is reflected in the increase, while the capacitive in the reduction of the impedance at the beginning. Of course, the value of the individual impact depends on the geometry of the GS, material properties, and structure of the soil and inclination of the current wave.

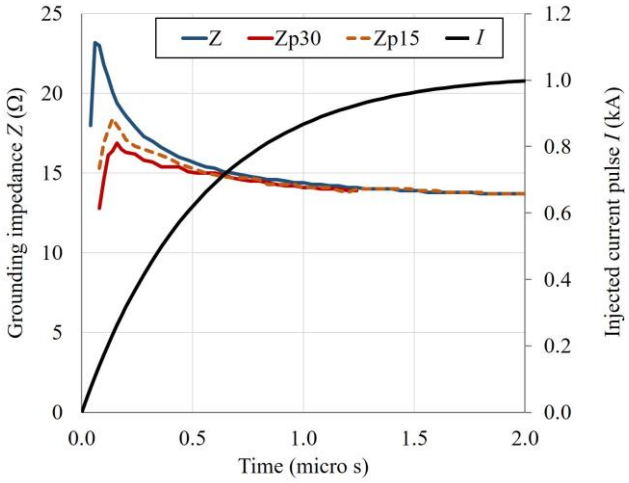

Fig. 13. Comparison between $Z(t)$ without and with considering the soil's permittivity.

B. Calculation with Consideration of the Soil Ionization

In Fig. 14 graphs $Z(t)$ are shown without and with consideration of the soil ionization, for three values of $\boldsymbol{E}_c$, which are 150 kV/m (Zi150), 450 kV/m (Zi450) and 750 kV/m (Zi750). It is clear from the graphs that the change in $Z(t)$ occurs only after a certain time, when the value of the initiated current increases to a value which, in the soil in the vicinity of the grounding electrodes causes increase of $\boldsymbol{E}$ over $\boldsymbol{E}_c$ or $\boldsymbol{J}$ over $\boldsymbol{J}_c$ and, thereby, initiates the ionization process. This is reflected in the decrease of the soil resistance in the continuation of the current pulse, which results in a decrease of $Z(t)$ until the ionization process is completed. Then $Z(t)$ begins (deionization process) to increase again. This section is not completely presented in the graphs. Additional consideration of the displacement current in the analysis of the soil ionization brings a change in value of $Z(t)$ only in the initial part of the graph. Since this is the same as on the graphs presented in Fig. 13, graphs for different permittivity are not added specifically. Figure 15 shows voltage U between mesh under test and auxiliary electrode for the mentioned conditions.

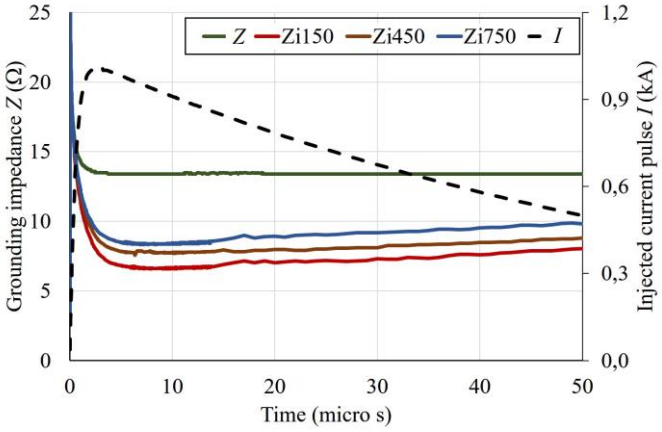

Fig. 14. Comparison between $Z(t)$ without and with considering the soil ionization effect

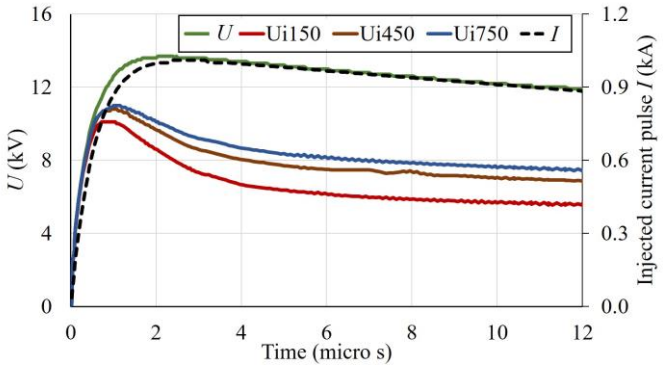

Fig. 15. Comparison between $U(t)$ without and with considering the soil ionization effect

Figure 16 shows the ionization/deionization region in the vicinity of the grounding mesh for a single time moment in combination with the electric potential distribution.

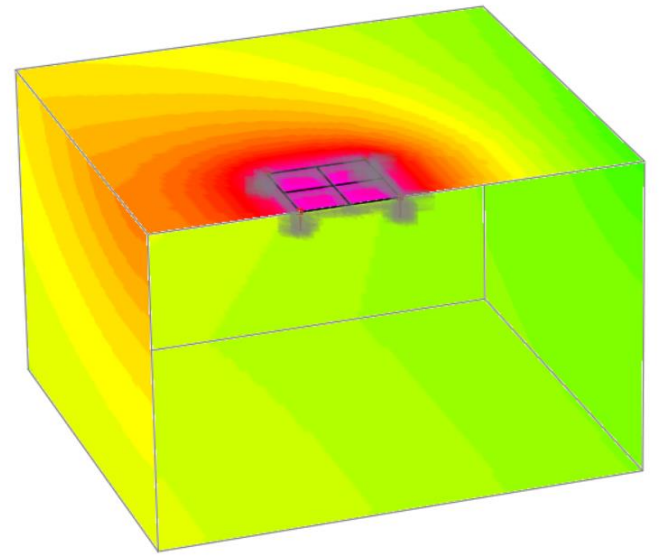

Fig. 16. Ionization/deionization region in the vicinity of the grounding mesh for E_c=150kV/m.

Of course, the distribution of the EMF is important in the analysis of the GS. Figure 17 shows the distribution of the electric potential on the surface and inside the soil. All graphs are made at the moment when the current reaches a peak value.

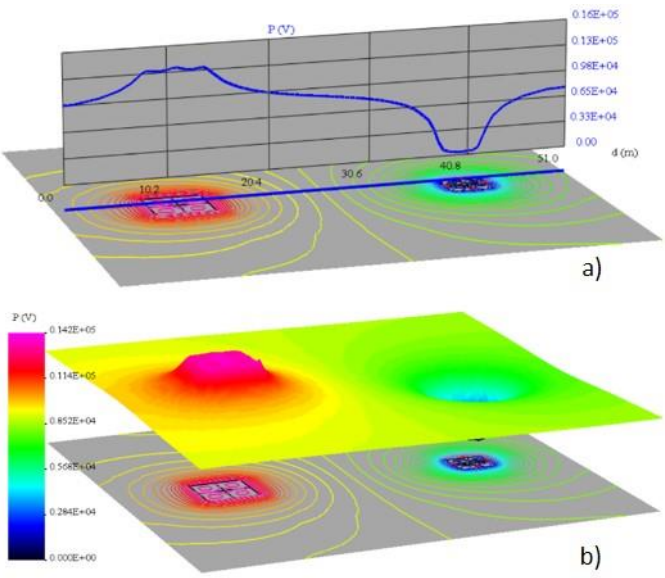

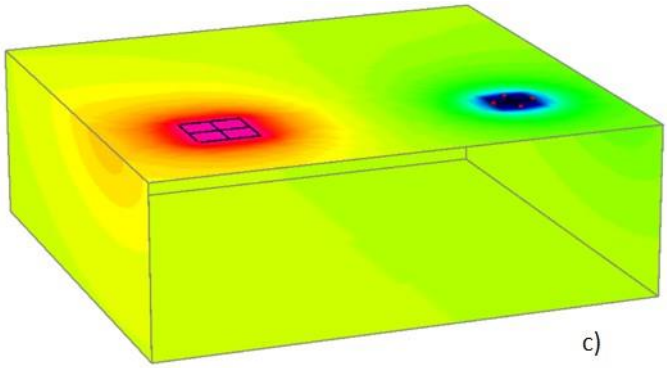

Fig. 17. Visualization of the electric potential; (a) 2D graph and equipotential lines on the surface, (b) 3D graph and equipotential lines on the surface, (c) color image of the potential distribution.

V. Conclusions

The article presents the use of the FEM for the calculation of the electromagnetic field in the vicinity of a GS in the case of a low frequency fault current, and in the case of a pulse shape current, as in the case of lightning discharge in the GS. Because soil is a really conductive material, for accurate calculation we also need accurate input data. These are conductivity, permittivity and permeability. Since the conductivity is not known for the entire discussed region, the soil in the calculation is replaced by an equivalent multilayer soil model, to which the conductivity and thickness of the layer are determined approximately by an experimental/numerical approach.

The permittivity of the soil is also approximate. The most accurate is the data for the permeability of the soil, for which we can take that $\mu=\mu_0$. This is important for the calculation results` implementation and for the selection of the method for GS analysis, especially when the ionization/deionization processes in the soil must be considered. Comparison of the graphs confirmed the effect of the soil, due to its conductivity, permittivity and dependence on $\boldsymbol{E}_c$ on the calculation results. It is important to note, that partial impact (conductive, inductive, capacitive and ionization effects) may be larger, smaller or negligible in certain cases. Of course, this is determined by the relations between conductivity, permittivity, $\boldsymbol{J}_c$, $\boldsymbol{J}_s$, and also the slope and the peak value of the current wave.

This means that, for a quality and credible analysis of the GS, a good knowledge of the GS problem is needed, and only “ad hoc” use of different software tools for the 3D calculation of EMF is not enough.

VI. References

[1] The IEEE Standards Association, “IEEE Guide for Safety in AC Substation Grounding”, *The IEEE Standards Association*, New York, 2000.

[2] IEEE Power and Energy Society, “IEEE Guide for Measuring Earth Resistivity, Ground Impedance, and Earth Surface Potentials of Grounding Systems”, *The Institute of Electrical and Electronics Engineering*, New York, 2012.

[3] O.C. Zienkiewicz, R.L. Taylor and J.Z. Zhu, “The Finite Element Method: its Basis and Fundamentals”, *Butterworth-Heinemann*, 2013.

[4] I.M. Smith and D.V. Griffiths, “Programing the Finite Element Method”, *Wiley&Sons, Ltd*, 2013.

[5] J. Katsikadelis, “The Boundary Element Method for Engineers and Scientists: Theory and Applications”, *Elsevier*, 2016.
[6] M. Kurtović and S. Vujević, “Numerical modeling of the earthing grid”, *Comput. Methods Eng., Adv. Applicat.*, 1, 869–874, 1992.
[7] A. Stochniol, “A general transformation for open boundary finite element method for electromagnetic problems”, *IEEE Transactions on Magnetics*, 28, 1679–1681, 1992.
[8] J. R. Cardoso, “FEM modeling of grounded system with unbounded approach”, *IEEE Transactions on Magnetics*, 30, 2893–2896, 1994.
[9] V. C. Silva, N. M. Abe, A. Passaro, and J. R. Cardoso, "A new line-element approach applied to 3D FEA of grounding systems", *7th International IGTE Symposium on Numerical Field Calculation in Electrical Engineering*, Proceedings, 410-415, 1996.
[10] M. Trlep, M. Hamler and B. Hribernik, “The analysis of complex grounding systems by FEM”, *IEEE Transactions on Magnetics*, 34, 2521–2524, 1998.
[11] M. Trlep, A. Hamler, M. Jesenik and B. Štumberger, "The FEM-BEM analysis of complex grounding systems", *IEEE Transactions on Magnetics*, 39, 1155-1158, 2003.
[12] A. Habjanič, M. Trlep, J. Pihler, "The Influence of an Additional Substance in the Trenches Surrounding the Grounding Grid’s Conductors on the Grounding Grid’s Performance", *IEEE Transactions on Magnetics*, 43, 1257-1260, 2007.
[13] M. Trlep, “FIELD_GS_low frequency”, V1.0”, *Internal Documentation, Applied Electromagnetics Laboratory*, 2012.
[14] T. Barič, D. Šljivac and M. Stojkov, “Validity limits of the expression for measuring soil resistivity by the Wenner method according to IEEE Standard 81-1983”, *Energija*, 56(3), 730-753, 2007.
[15] A.E. Eiben and J.E. Smith, “Introduction to Evolutionary Computing”, *Springer*, Heidelberg, Germany, 2008.
[16] D. Karaboga and B. Basturk, “On The Performance Of Artificial Bee Colony (ABC) Algorithm”, *Applied Soft Computing*, 8(1), 687-697, 2008.
[17] J. Brest, A. Zamuda, B. Boškovič, M.S. Maučec and V. Žumer, “Dynamic Optimization using Self-Adaptive Differential Evolution”, *IEEE Congress on Evolutionary Computations*, 415-422, 2009.
[18] W.P. Calixto, L.M. Neto, M. Wu, K. Yamanaka and E. Moreira, “Parameters Estimation of Horizontal Multilayer Soil Using Genetic Algorithm”, *IEEE Transactions on Power Delivery*, 25(3), 1250-1257, 2010.
[19] R.V. Rao, V.J. Savsani and D.P. Vakharia, “Teaching-learning-based optimization: A novel method for constrained mechanical design optimization problems”, *Computer-Aided Design*, 43, 303-315, 2011.
[20] M.J. Kang, C.J. Boo, H.C. Kim and J.M. Zurada, “A Nonlinear Regression based Approach for Multilayer Soil Parameter Estimation”, *International Journal of Control and Automation*, 7(2), 65-74, 2014.
[21] W.R. Pereira, M.G. Soares and L.M. Nato, “Horizontal Multilayer Soil Parameter Estimation Through Differential Evolution”, *IEEE Transactions on Power Delivery*, 31(2), 622-629, 2016.
[22] M. Jesenik, M. Beković, A. Hamler and M. Trlep, “Analytical modelling of a magnetization curve obtained by the measurements of magnetic materials’ properties using evolutionary algorithms”, *Applied Soft Computing*, 52, 387-408, 2017.
[23] M. Jesenik, M. Mernik, M. Črepinšek, M. Ravber and M. Trlep, “Searching for soil models’ parameters using metaheuristics”, *Applied Soft Computing*, 69, 131-148, 2018.
[24] O. Biro and K. Preis, "On the use of the magnetic vector potential in the finite element analysis of the three dimensional eddy current", *IEEE Transactions on Magnetics*, 25(4), 3145-3159, 1989.
[25] L. Grcev and F. Dawalibi, "An electromagnetic model for transients in grounding systems", *IEEE Transactions on Power Delivery*, 5(4), 1773-1781, 1990.
[26] G. Ala and M. L. Di Silvestre, “A simulation model for electromagnetic transients in lightning protection systems”, *IEEE Transactions on Electromagnetic Compatibility*, 44(4), 539–554, 2002.
[27] Y. Liu, “Transient response of grounding systems caused by lightning: modelling and experiments”, *Ph.D. dissertation, Faculty of Science and Technology, Univ. Uppsala*, 2004.
[28] Y. Liu, N. Theethayi and R. Thottappillil, “An Engineering Model for Transient Analysis of Grounding System under Lightning Strikes: Non uniform Transmission-Line Approach”, *IEEE Transactions on Power Delivery*, 20(2), 722-730, 2005.
[29] D. Poljak and V. Doric, “Wire antenna model for transient analysis of simple grounding systems, part I: the vertical grounding electrode”, *Progress Electromagnetic Research*, 64, 149-166, 2006.
[30] L. Grcev, “Impulse Efficiency of Ground Electrodes”, *IEEE Trans. on Power Delivery*, 24(1), 441-451, 2009.
[31] N. Ramezani and S.M. Shahrtash, “Calculating the transient behavior of grounding systems using inverse Laplace transform”, *Computers & Electronics*, 12(3), 250-262, 2011.
[32] M. Trlep, M. Jeseni and A. Hamler, “Transient calculation of electromagnetic field for grounding system based on consideration of displacement current”, *IEEE Transactions on Magnetics*, 48(2), 207-210, 2012.
[33] N.N. Mohamad, M. Trlep, S. Abdullah and R. Rajab, “Investigations of earthing systems under steady-state and transients with FEM and experimental work”, *International journal of electrical power & energy systems*, 44(1), 758-763, 2013.
[34] B. Nekhoul, D. Poljak, D. Sekki, D. Cavka, B. Harrat, K. Kerroumc, K.El. Khamlichi Drissi, “An efficient transient analysis of realistic grounding systems: Transmission line versus antenna theory approach”, *Engineering Analysis with Boundary Elements*, 48, 14-23, 2014.
[35] A. Ametani and all (members), Y.Baba (corresponding member), “Guideline for Numerical Electromagnetic Analysis Method and its Application to Surge Phenomena”, *Cigre WG C4.501*, 2013.
[36] M. Trlep, “FIELD_GS_transient V1.0”, *Internal Documentation, Applied Electromagnetics Laboratory*, 2013.
[37] Z. Stojković, M.S. Savić, J.M. Nahman, D. Salamon and B. Bukorović, "Sensitivity Analysis of Experimentally Determined Grounding Grid Impulse Characteristics", *IEEE Trans. on Power Delivery*, 13(4), 1136-1141, 1998.
[38] C. M. Portela, J. B. Gertrudes, M. C. Tavares and J. Pissolato, “Earth Conductivity and Permittivity Data Measurements: Influence in Transmission Line Transient Per- formance”, *Elsevier, Electric Power Systems Research*, 76(11), 907-915, 2006.
[39] M.A.O. Schroeder1, M.M. Afonso, T.A.S. Oliveira and S.C. Assis, “Computer Analysis of Electromagnetic Transients in Grounding Systems Considering Variation of Soil Parameters with Frequency”, *Journal of Electromagnetic Analysis and Applications*, 4, 475-480, 2012.

[40] S. Visacro and R. S. Alípio, “Frequency Dependence of Soil Parameters: Experimental Results, Predicting Formula and Influence on the Lightning Response of Grounding Electrodes”, *IEEE Transactions on Power Delivery*, 27(2), 927-935, 2012.

[41] Z.-X. Li, Y. Yin, C.-X. Zhang and L.-C. Zhang, “Frequency dependent characteristics of grounding system buried in multilayered earth model based on quasi-static electromagnetic field theory”, *Progress In Electromagnetics Research*, 33, 169–183, 2013.

[42] E. Garbagnati, A. Geri, G. Sartorio, and G. M. Veca, “Non-linear behavior of ground electrodes under lightning surge currents: Computer modeling and comparison with experimental results,” *IEEE Transactions on Magnetics*, 28(2), 1442–1445, 1992.

[43] A.M. Mousa, “The soil ionization gradient associated with discharge of high currents into concentrated electrodes”, *IEEE Transactions on Power Delivery*, 9(3), 1669-1677, 1994.

[44] A. Geri, “Behaviour of grounding systems excited by high impulse currents: The model and its validation”, *IEEE Transactions on Power Delivery*, 14(3), 1008–1017, 1999.

[45] A. Habjanič and M. Trlep, “The simulation of the soil ionization phenomenon around the grounding system by the finite element method”, *IEEE Transactions on Magnetics*, 42(4), 867-870, 2006.

[46] A.C. Liew and M. Darveniza, “Dynamic model of impulse characteristics of concentrated earths”, *Proc. IEE*, 121(2), 123–135, 1974.

[47] Y. Liu, N. Theethayi, R. Thottappillil, R.M. Gonzales and M. Zitnik, “An improved model for soil ionization around grounding system and its application to stratified soil”, *Journal of Electrostatics*, 60(2-4), 203–209, 2004.

[48] A.C. Liew, J. Wang and M. Darveniza, “Extension of dynamic model of impulse behaviour of concentrated earths at high currents”, *IEEE Transactions on Power Delivery*, 20(3), 2160– 2165, 2005.

[49] J. Wang, A.C. Liew and M. Darveniza, “Extension of Dynamic Model of Impulse Behavior of Concentrated Grounds at High Currents”, *IEEE Transactions on Power Delivery*, 20(3), 2160-2165, 2005.

[50] B. Zhang, J. He, J.-B. Lee, X. Cui, Z. Zhao, J. Zou and S.-H. Chang, “Numerical analysis of transient performance of grounding systems considering soil ionization by coupling moment method with circuit theory”, *IEEE Transactions on Magnetics*, 41(5), 1440–1443, 2005.

[51] S. Sekioka, M.I. Lorentzou, M.P. Philippakou and J.M. Prousalidis, “Current-Dependent Grounding Resistance Model Based on Energy Balance of Soil Ionization”, *IEEE Transactions on Power Delivery*, 21(1), 194-201, 2006.

[52] G. Ala, P.L. Buccheri, P. Romano and F. Viola, “Finite difference time domain simulation of earth electrodes soil ionization under lightning surge condition”, *IET Science, Measurement and Technology*, 2(3), 134–145, 2008.

[53] R. Zeng, X. Gong, J. He, B. Zang and Y. Gao, “Lightning impulse performance of grounding grids for substations considering soil ionization”, *IEEE Transactions on Power Delivery*, 23(2), 667–675, 2008.

[54] G. Ala, M.L.D. Silvestre and F. Viola, “Soil Ionization Due to High Pulse Transient Currents Leaked by Earth Electrodes”, *Progress in Electromagnetics Research B*, 14, 1–21, 2009.

[55] T.L.T. dos Santos, R.M.S. de Oliveira, C.L. da S.S. Sobrinho and J.F. Almeida, “Ionization in Different Types of Grounding Grids Simulated by FDTD Method”, *SBMO/IEEE MTT-S International Microwave & Optoelectronics Conference IMOC*, 127-132, 2009.

[56] R.R. Diaz and J.N. Silva, “Space Charge and Soil Ionization: An Electro-kinetic Approach”, *IEEE Transactions on Dielectrics and Electrical Insulation*, 18(6), 2032-2039, 2011.

[57] B. Zhang, J. Wu, J. He and R. Zeng, “Analysis of Transient Performance of Grounding System Considering Soil Ionization by Time Domain Method”, *IEEE Transactions on Magnetics*, 49(5), 1837-1840, 2013.

[58] K. Otani, Y. Baba, A. Ametani, Y. Shiraki, N. Nagaoka and N. Itamoto, “FDTD Simulation of Grounding Electrodes Considering Soil Ionization”, *Electric Power Systems Research*, 113, 171–179, 2014.

[59] D.S. Gazzana, A.S. Bretas, G.A.D. Dias, M. Telló, D.W.P. Thomas and C. Christopoulos, “The Transmission Line Modeling Method to Represent the Soil Ionization Phenomenon in Grounding Systems”, *IEEE Transactions on Magnetics*, 50(2), 7012404, 2014.

[60] Z. Feng, X. Wen, X. Tong, H. Lu, L. Lan and P. Xing, “Impulse Characteristics of Tower Grounding Devices Considering Soil Ionization by the Time-Domain Difference Method”, *IEEE Transactions on Power Delivery*, 30(4), 1906-1913, 2015.

[61] J. He and B. Zhang, “Progress in Lightning Impulse Characteristics of Grounding Electrodes with Soil Ionization”, *IEEE Transactions on Industry Applications*, 51(6), 4924-4933, 2015

[62] V.L. Coelho, L.F. Venturini, A. Piantini, H.A.D. Almaguer, R.A. Coelho, W.C. Boaventura, J.O.S. Paulino and P.L. Nosaki, “Soil Resistivity Behavior under High Current Density Values Using the Energy Balance Method”, *International Symposium on Lightning Protection*, Balneario Camboriu, Brasil, 129-136, 2015.

[63] W. Sima, S. Liu, T. Yuan, D. Luo, P. Wu and B. Zhu, “Experimental Study of the Discharge Area of Soil Breakdown under Surge Current Using X-Ray Imaging Technology”, *IEEE Transactions on Industry Applications*, 51(6), 5343-5351, 2015.

[64] D.S. Gazzana, B. A.B. Tronchoni, R.C. Leborgne, A.S. Bretas, D.W.P. Thomas and C. Christopoulos, “An Improved Soil Ionization Representation to Numerical Simulation of Impulsive_Grounding Systems”, *IEEE Transactions on Magnetics*, 54(3), 2018.

[65] P. Espel, R.R. Diaz, A. Bonamy and J.N. Silva, “Electrical Parameters Associated with Discharges in Resistive Soils”, *IEEE Transactions on Power Delivery*, 19(3), 1174-1182, 2004.

[66] N.M. Nor, A. Haddad and H. Griffiths, “Characterization of Ionization Phenomena in Soils under Fast Impulses”, *IEEE Trans. on Power Delivery*, 21(1), 353-360, 2006.

[67] F.E. Asimakopoulou, I.F. Gonos and I.A. Stathopulos, Methodologies for determination of soil ionization gradient”, *Journal of Electrostatics*, 70, 457-461, 2012.

[68] N.M. Nor, M. Trlep, S. Abdullah, R. Rajab and K. Ramar, “Determination of threshold electric field of practical earthing systems by FEM and experimental work”, *IEEE Transactions on Power Delivery*, 28(4), 2180-2184, 2013.

AUTHORS NAMES AND AFFILIATIONS

Mladen Trlep, Anton Hamler, Marko Jesenik, Miloš Beković, Viktor Goričan, Applied Electromagnetics Laboratory, Faculty of Electrical Engineering and Computer Science, University of Maribor, Koroška cesta 46, 2000 Maribor, Slovenia.

Corresponding author: Mladen Trlep (mladen.trlep@um.si)